Modeling of concentrating solar thermoelectric generators

Citation: McEnaney, Kenneth et al. "Modeling of Concentrating Solar Thermoelectric Generators." Journal of Applied Physics 110.7 (2011): 074502. © 2011 American Institute of Physics

As Published: http://dx.doi.org/10.1063/1.3642988

Publisher: American Institute of Physics (AIP)

Persistent URL: http://hdl.handle.net/1721.1/78253

Version: Final published version: final published article, as it appeared in a journal, conference proceedings, or other formally published context

AIP | Journal of Applied Physics

Modeling of concentrating solar thermoelectric generators

Kenneth McEnaney, Daniel Kraemer, Zhifeng Ren, and Gang Chen

Citation: J. Appl. Phys. **110**, 074502 (2011); doi: 10.1063/1.3642988
View online: http://dx.doi.org/10.1063/1.3642988
View Table of Contents: http://jap.aip.org/resource/1/JAPIAU/v110/i7
Published by the American Institute of Physics.

Modeling of concentrating solar thermoelectric generators

Kenneth McEnaney,[1] Daniel Kraemer,[1] Zhifeng Ren,[2] and Gang Chen[1,a)]
[1]*Department of Mechanical Engineering, Massachusetts Institute of Technology, Cambridge, Massachusetts 02139, USA*
[2]*Department of Physics, Boston College, Chestnut Hill, Massachusetts 02467, USA*

(Received 27 July 2011; accepted 20 August 2011; published online 3 October 2011)

The conversion of solar power into electricity is dominated by non-concentrating photovoltaics and concentrating solar thermal systems. Recently, it has been shown that solar thermoelectric generators (STEGs) are a viable alternative in the non-concentrating regime. This paper addresses the possibility of STEGs being used as the power block in concentrating solar power systems. STEG power blocks have no moving parts, they are scalable, and they eliminate the need for an external traditional thermomechanical generator, such as a steam turbine or Stirling engine. Using existing skutterudite and bismuth telluride materials, concentrating STEGs can have efficiencies exceeding 10% based on a geometric optical concentration ratio of 45. © *2011 American Institute of Physics*. [doi:10.1063/1.3642988]

I. INTRODUCTION

Due to rising petroleum costs, as well as environmental and security concerns, much research is being directed toward harvesting the energy of the sun. The two most commonly studied technologies are solar photovoltaics and solar thermal power plants. One technology that has received only sporadic attention is solar thermoelectrics. Thermoelectrics are materials which generate a voltage in the presence of a temperature gradient.[1] When these materials are sandwiched between a solar absorber and a heat sink to establish a temperature difference and generate power, they are called solar thermoelectric generators (STEGs), converting solar power to electric power. Like solar thermal plants, these generators have the advantage that they can use the entire solar spectrum, not just the portion above the bandgap of a semiconductor. Like photovoltaics, STEGs can be used for small-scale installations, as they do not require a traditional thermomechanical generator like solar thermal systems. Because STEGs are solid-state devices, they have no moving parts, which increases reliability and reduces maintenance.

Using thermoelectric materials to capture the sun's energy is not a new concept; the first patent for a solar generator made from thermoelectric materials was in 1888.[2] In 1954, Telkes reported 0.6% efficiency at one sun and 3.3% efficiency at 50 suns.[3] Prior to 2010, a few studies have investigated solar thermoelectric generators, but none made significant improvement over Telkes' work.[4–7] Recently, we have demonstrated an efficiency of over 4% for a non-optically concentrating solar thermoelectric generator,[8] matching modeling predictions.[9,10] This leap in efficiency can be attributed to (1) vacuum operation that enables a large concentration of solar energy via heat conduction, i.e., thermal concentration, (2) selective surfaces that absorb solar radiation with small thermal emission, and (3) better thermoelectric materials.[11] The relevant metrics for these individual components are the absorptance and emittance of spectrally selective absorbers and the dimensionless figure of merit of thermoelectric materials, $ZT = S^2\sigma T/\kappa$, where S is the Seebeck coefficient, σ the electrical conductivity, T the absolute temperature, and κ the thermal conductivity. Significant advances have been made over the last few decades in thermoelectric materials.[12–14]

For systems without optical concentration, the optimal hot-side operational temperature of the STEG is near 200 °C.[8] Although a higher temperature can lead to a higher thermoelectric device efficiency, radiation heat loss from the large absorber surface reduces the thermal efficiency. Although Bi_2Te_3-based materials, which operate up to 200 °C, are available, materials with good ZT at higher temperatures are also available, such as skutterudites[15] and half-Heuslers.[16] Optical concentration can be employed together with thermal concentration to reduce the absorber area and increase the system efficiency. The efficiency of earth-based concentrating STEGs has been predicted to be as high as 12% for a theoretical silicon-germanium material at a concentration of nearly 2000 suns.[17] This article builds off the recent advances in non-concentrating solar thermoelectric generators[8–10] and examines the potential performance for concentrating STEGs using existing selective surfaces and thermoelectric materials. We predict an efficiency equaling that from Rowe,[17] but with an optical concentration of 50 instead of 2000.

II. MODEL

A concentrating solar thermoelectric generator comprises an optical concentration system, a glass enclosure, an absorber, a thermoelectric generator (TEG), and a heat sink. The glass enclosure, which envelops the absorber and the TEG, is used to maintain a vacuum to reduce thermal losses and to reduce contamination or oxidation of the absorber and TEG. The absorber converts the concentrated solar radiation into thermal energy of the absorber. This thermal energy can be concentrated via heat conduction to the thermoelectric generator, which converts the heat into electricity. The excess heat is removed by the heat sink. The efficiency of a

a)Author to whom correspondence should be addressed. Electronic mail: gchen2@mit.edu.

STEG is defined as the amount of electric power produced per unit of intercepted solar power, $\eta_{steg} = P_{el}/(H_{ap}A_{ap})$, where P_{el} is the total electric power produced by the STEG, H_{ap} is the solar irradiation at the aperture of the concentrator, and A_{ap} is the aperture area of the concentrator. The STEG efficiency is the product of the opto-thermal efficiency and the TEG efficiency, $\eta_{steg} = \eta_{ot}\eta_{teg}$, where the opto-thermal efficiency characterizes the conversion of solar flux into a heat flux at the hot junction of the TEG and the TEG efficiency characterizes the conversion of heat into electricity.[3]

The optical concentration system for most solar energy converters is either a mirror-based or lens-based concentrator. These systems have two reference areas: the aperture area, A_{ap}, which sets the total amount of sunlight intercepted by the system, and the absorber area, A_{abs}, which is the area of the absorber surface which absorbs the sunlight for conversion to electricity. The ratio of these two areas gives a geometric optical concentration, $C_{g,opt}$. The energy flux will be concentrated by a factor smaller than the optical concentration because of mirror or lens losses. The aperture flux is taken as the AM 1.5 direct + circumsolar flux,[18] since diffuse light cannot be concentrated. The specific design of optical concentrators is not discussed in this paper.

Just as an optical concentrator can increase the heat flux by channeling a diffuse source into more concentrated flux, a thermal concentrator can increase the heat flux by directing the heat to flow through an area of smaller cross-section. Thermal concentration allows higher temperatures to be reached while minimizing the amount of thermoelectric materials needed.[10] Analogous to optical concentration, thermal concentration can be defined by a geometric thermal concentration, $C_{g,th}$, which is the ratio of the absorber area to the TEG cross-sectional area.

A steady-state energy balance on the absorber details the losses which limit the thermal efficiency,

$$Q_{teg,in} = Q_{abs,ss} - Q_{r,ss} - Q_{r,edge} - Q_{r,back} - Q_{c,ss} - Q_{c,edge} - Q_{c,back}. \quad (1)$$

Here, $Q_{teg,in}$ is the heat conducted into the top of the TEG; $Q_{abs,ss}$ is the heat absorbed by the selective surface; $Q_{r,ss}$, $Q_{r,edge}$, and $Q_{r,back}$ are the heat losses via radiation from the absorber's selective surface, edges, and back side; and $Q_{c,ss}$, $Q_{c,edge}$, and $Q_{c,back}$ are the heat losses via conduction or convection from the absorber's selective surface, edges, and back side. To minimize losses, the system can be placed in a vacuum enclosure such that the last three terms, the air conduction/convection losses, are eliminated. The radiation losses from the selective surface and from the edges of the absorber can be estimated by assuming a view factor of 1 to the blackbody surroundings at the temperature T_{amb}, although measures can be taken to reduce this loss. The first three heat flow terms of Eq. (1) can be expressed as

$$Q_{abs,ss} = \alpha_{ss}H_{abs}A_{abs}, \quad (2)$$

$$Q_{r,ss} = \sigma\varepsilon_{ss}A_{abs}(T_{abs}^4 - T_{amb}^4), \quad (3)$$

$$Q_{r,edge} = \sigma\varepsilon_{edge}A_{edge}(T_{abs}^4 - T_{amb}^4). \quad (4)$$

Here, α_{ss} is the absorptance of the selective surface in the solar spectrum; H_{abs} is the incident radiative flux on the absorber; A_{abs} and A_{edge} are the areas of the absorber selective surface and the absorber edge; σ is the Stefan-Boltzmann constant; ε_{ss} and ε_{edge} are the effective emittances of the selective surface and absorber edge at the absorber temperature, T_{abs}; and T_{amb} is the temperature of the surroundings. Such effective emittances may depend on the properties of the enclosure, for example. The radiative loss from the back side of the absorber, $Q_{r,back}$, is dependent on the temperature, emittance, and view factor of the ambient and the surface facing the back side. The facing surface is the cold-junction electrodes for a single-stage TEG (Fig. 1). To solve for the radiation losses, a three-body radiation network[19] must be solved between the back side of the absorber, the top of the cold side, and the gap between the two. This gap can be treated as a blackbody at the temperature of the surroundings. The surfaces of the thermoelectric

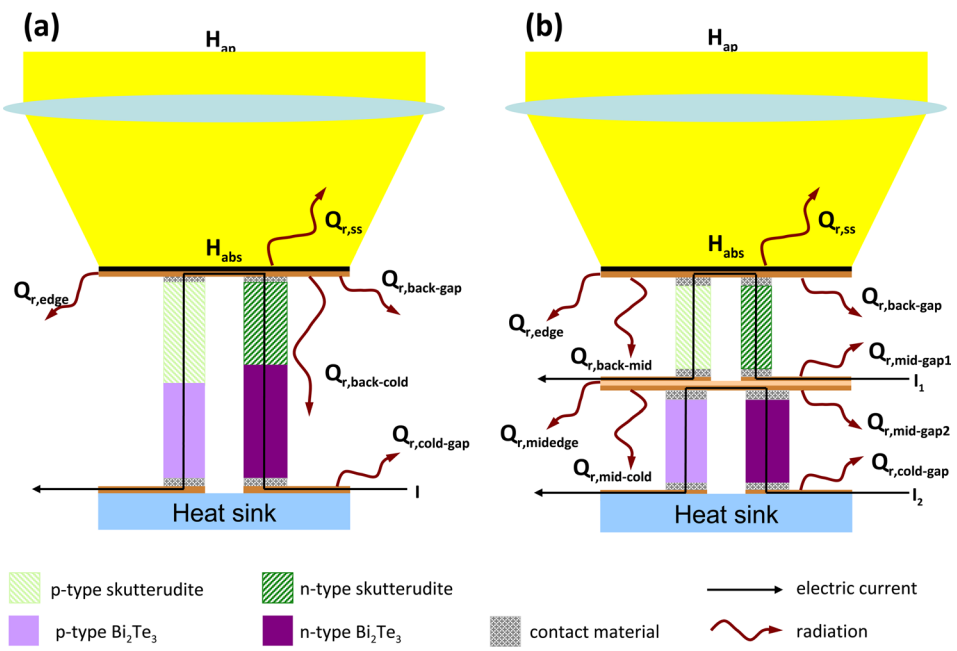

FIG. 1. (Color online) Schematic of two basic STEG architectures: (a) segmented and (b) cascaded STEGs. The copper absorber substrate is also used as the electrical connection between the *p*-type and *n*-type legs. The cascaded architecture uses a midplane with an electrically insulating core to separate the two electric circuits.

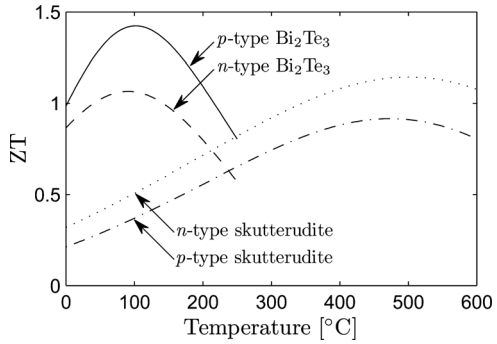

FIG. 2. *ZT* of materials used in these calculations. Lower-temperature *n*-type (dashed) and *p*-type (solid) Bi_2Te_3 materials and higher-temperature *n*-type (dotted) and *p*-type (dash-dotted) skutterudites.

elements are neglected in the radiation exchange model because of their relatively small size compared to that of the gap.

Of the heat that is transported into the TEG, only a small portion is converted into electricity. The TEG, being a heat engine, is limited in its efficiency by the second law of thermodynamics. In addition, the materials' *ZT* depends strongly on temperature. For generators operating over a large temperature range, usually several materials are combined together to maximize the efficiency of the system. In Fig. 2, we show the *ZT* of two materials studied in this paper.[11,15] Bi_2Te_3-based materials have higher *ZT* at low temperatures, while skutterudites have higher *ZT* over a higher temperature range. Our previous STEG demonstration used little optical concentration, resulting in a lower operating temperature, for which Bi_2Te_3-based materials worked well. For optically concentrating systems that can operate at higher temperatures, we are interested in the achievable STEG efficiency.

Two main architectures for multi-material thermoelectric generators are cascaded[20] and segmented[21] generators. These architectures are shown integrated into a STEG in Fig. 1. A segmented generator looks superficially similar to a single-stage TEG, in that there is only one electric circuit in the device and the thermoelectric legs run all the way from the hot side to the cold side. Each leg is composed of a skutterudite upper segment joined to a bismuth telluride lower segment. The second architecture, a cascaded generator, has a skutterudite stage with its own electric circuit placed on top of a bismuth telluride stage with its own electric circuit. The two stages are separated by a thermally conducting, electrically insulating midplane. The two separate currents in this architecture give an extra degree of freedom for optimizing the performance of the TEG. In contrast, although the segmented generator has only one electric circuit, there is an extra degree of freedom provided by the fact that the transition from skutterudite to bismuth telluride can happen at a different temperature in the *n*-type leg than in the *p*-type leg, whereas this transition temperature is the single midplane temperature for a cascaded generator.

To analyze the operation of a TEG, the governing equations for thermoelectric materials[22] must be solved. Assuming the heat flux and electric current can be considered one-dimensional conserved quantities inside the thermoelectric materials, a steady-state energy balance on a differential slice of a single thermoelectric element is shown in Fig. 3. The three terms are the Fourier heat flux, the thermoelectric heat flux, and the electric power flux. This energy balance reduces to a single differential equation for the temperature profile in the element (Eq. (5)),

$$\frac{\partial}{\partial x}\left(\kappa(x)\frac{\partial T(x)}{\partial (x)}\right) = -\rho J^2 + JT(x)\frac{\partial S(x)}{\partial x}, \tag{5}$$

which can be solved via an iterative technique by breaking the equation into a set of coupled differential equations (Eqs. (6) and (7)).[23]

$$\frac{dT}{dx} = \frac{TSJ - q}{\kappa}, \tag{6}$$

$$\frac{dq}{dx} = \rho J^2 + SJ\frac{TSJ - q}{\kappa}. \tag{7}$$

These equations can be solved numerically for a thermoelectric element to find the temperature distribution and heat flux profile within the element, as well as the power output and efficiency of the element. This basic framework for determining the performance of a thermoelectric element can be incorporated into finding the efficiency of a TEG with multiple thermoelectric elements, either in a single-stage, segmented, or cascaded architecture.

The full model for a segmented concentrating STEG is presented in Fig. 1(a) (other device geometries are possible,[24] but the optimization concept is the same). The efficiency of the STEG is maximized by varying the electric current through the system as well as all the dimensions of the individual segments and the absorber; the only geometric constraint in this configration is that the total length of each

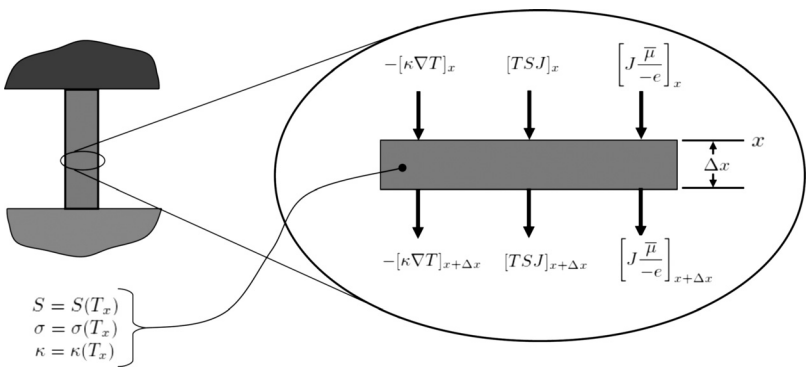

FIG. 3. Energy balance on a differential thermoelectric element. The material properties are a function of the local temperature, and energy is conserved in the *x*-direction. The three terms are the Fourier heat, the thermoelectric heat, and the electrical power. Here *J* is the electric current density, $\bar{\mu}$ the electrochemical potential, and $-e$ the charge of an electron.

leg is the same. The temperature of the absorber is not fixed, but is calculated from the energy balance in Eq. (1). The full model includes bonding agents, such as solder, and also takes into account both thermal and electrical contact resistance at the interfaces. For the purposes of predicting an upper limit for the efficiency, the solder is ignored and all contact resistances are set to zero.

A cascaded STEG is represented schematically in Fig. 1(b). Because of the midplane, two different three-body radiation networks must be solved: one consisting of the back side of the absorber, the top of the midplane, and the upper gap and a second network consisting of the bottom of the midplane, the lower gap, and the top of the cold side. The heat input into the bottom TEG, $Q_{teg2,in}$, is the heat that leaves the bottom of the upper TEG, $Q_{teg1,out}$, less the net radiation loss from the midplane,

$$Q_{teg2,in} = Q_{teg1,out} + Q_{r,back-mid} - Q_{r,mid-gap1} - Q_{r,mid-gap2} - Q_{r,mid-cold} - Q_{r,midedge} - Q_{c,wire}, \quad (8)$$

where $Q_{c,wire}$ is the conduction losses down any wires that are part of the upper TEG electric circuit. Snyder[25] has shown that these wires can be eliminated through clever design of the upper and lower TEG circuit paths, so here, the wire conduction losses will be ignored.

In these models, it is assumed that the absorber is at a uniform temperature, T_{abs}. In reality, this will not be the case because of the temperature drop caused by the radial conduction from the edges of the absorber to the junction with the TEG. Since it has been shown that these effects are negligible under most circumstances, even for STEGs with large thermal concentration,[10] this assumption is valid for the smaller thermal concentration required by high optical concentration systems, as long as the copper absorber substrate is of sufficient thickness. The radiation from the absorber to a thermoelectric element is neglected because the magnitude of that radiation exchange is small compared to the total heat conducted down the leg. Similarly, the radiation from one leg to other legs or to the gap is neglected because of the small magnitudes of these radiation losses compared to the magnitude of the conducted heat. For large numbers of closely packed legs, the radiation effects are usually small, but this assumption should be tested for a given temperature range and approximate system geometry. Neglecting the radiation exchange involving the legs drastically reduces the computation time to run these simulations and allows the program to be modular.

This model was run to calculate the maximum efficiency of a STEG under 1 to 1000 times geometric optical concentration. The mirror reflectance was assumed to be 0.96, and the concentrator intercept factor[26] was 0.92. The average transmittance of the glass tube is 0.9, and the commercially available absorber has 94% absorption in the solar spectrum. It is assumed that the efficiency of the optical system is independent of wavelength such that it would still be valid to use the manufacturer's data for the selective surface's absorptance in the solar spectrum for the absorptance of the spectrum incident on the absorber. This leads to an average irradiance on the absorber of 0.67 kW/m^2 to 670 kW/m^2.

TABLE I. Individually optimized *p*- and *n*-type segmented thermoelectric legs.

	p-type		*n*-type
T_h [°C]		400	
T_{mid} [°C]	241		211
T_c [°C]		20	
Skutterudite efficiency	3.5%		4.9%
Bi_2Te_3 efficiency	10.0%		7.7%
Leg efficiency	13.2%		12.2%
TEG efficiency		12.7%	

The selective surface has an emittance that increases from 4% emittance at 100 °C to 20% at 600 °C. The back side of the absorber, both midplane faces, and the upper surface of the cold side were all assumed to be highly polished copper with a temperature-independent emittance of 4%. Edge effects were neglected because, as the system is scaled up to many pairs, the relative size of the edges decreases and, thus, the edge losses become unimportant. The thermoelectric materials were bismuth telluride compounds for the lower stage and skutterudites for the upper stage. The bismuth telluride *p*-type elements peak at a *ZT* of nearly 1.4 at 100 °C,[11] and the *ZT* of the *n*-type skutterudites peaks above 1 at 500 °C.[15]

III. RESULTS AND DISCUSSION

The model was first run without the solar component in order to make a comparison between single-stage, segmented, and cascaded TEGs. Simulations calculated the efficiency of the TEGs as a function of the hot-side temperature, assuming the cold side was fixed at 20 °C. As an example, the optimized system parameters for a skutterudite and bismuth telluride segmented TEG operating between 400 °C and 20 °C are presented in Table I. The results for a cascaded TEG under the same conditions and made of the same materials are shown in Table II. Note that the bismuth telluride efficiency is defined based on the heat flux into the bismuth telluride portion; because of this, the total efficiency must be lower than the sum of the skutterudite and bismuth telluride efficiencies.

From Table I, it is clear that, at the optimal performance of the device, the temperature at the transition from skutterudite to bismuth telluride is different in each leg. Because of the midplane used in the cascaded model, the transition temperatures in both legs are the same. The cascaded midplane temperature does not match either segmented transition temperature because that temperature is optimized for two

TABLE II. Performance of a cascaded thermoelectric generator.

T_h [°C]	400
T_{mid} [°C]	210
T_c [°C]	20
Skutterudite efficiency	4.8%
Bi_2Te_3 efficiency	8.6%
TEG efficiency	13.0%

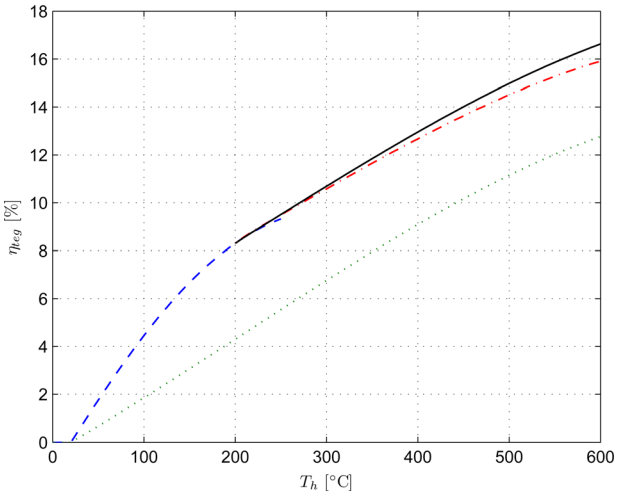

FIG. 4. (Color online) TEG efficiency for four different architectures: a single-stage bismuth telluride TEG (dashed); a single-stage skutterudite TEG (dotted); a segmented skutterudite and bismuth telluride TEG (dash-dotted); and a cascaded skutterudite and bismuth telluride TEG (solid).

different currents in the system. Specifically, because bismuth telluride is not as self-compatible as skutterudites, the current is biased toward the mean value for bismuth telluride.[27] With this as the current in the device, the bismuth telluride material is more efficient than skutterudites for a larger temperature range.

Figure 4 shows the efficiencies of different TEG architectures: single-stage bismuth telluride, single-stage skutterudites, segmented bismuth telluride/skutterudite legs, and cascaded bismuth telluride/skutterudite TEGs. Since these results are just the TEG efficiency, the effects of radiation between surfaces are not included. When the hot-side temperature is below 200 °C, there is no benefit from adding a skutterudite section above the bismuth telluride section. At temperatures above 200 °C, a cascaded TEG is more efficient than a segmented TEG. These two architectures each have a different extra degree of freedom: the segmented architecture allows the *p*-type leg and *n*-type leg transition temperatures to be different, while the cascaded architecture allows two different currents to be run in the TEG. Because the transition temperatures of the *p*-type and *n*-type legs are not far apart, the larger efficiency comes from exercising the two-current degree of freedom.

The optimization of cascaded and segmented TEGs is made much simpler when contact resistances and losses from the leg surfaces are ignored and the heat flow is treated as one-dimensional because, under these conditions, the element efficiency is independent of geometry. The end temperatures and the relative current density[27] fully define the efficiency of the thermoelectric element.[28] For segmented TEG legs, the transition temperature from one segment to the next is defined by the relative thermal resistances of each segment, which are proportional to the length over the area of each segment. For ease of manufacturing, the areas of both segments of the leg can be made equal, and then it is just the ratio of the lengths of the segments that controls the transition temperature. A single leg of a TEG can therefore be optimized by choosing a leg cross-sectional area and a total leg length and only varying the electric current and the location along the leg where the transition occurs from one material to the next. The efficiency will stay the same as long as the leg fractions and the length-weighted current density, IL/A, remain constant. This eliminates many of the variables in the optimization, resulting in a much more clear picture of the concept of segmented thermoelectric generators.

Once a single leg has been optimized, the optimization of a pair of legs is straightforward:[29,30] the ratio of the cross-sectional areas of the *n*-type and *p*-type leg is adjusted until the efficiency of the STEG is maximized. This pair can then be incorporated into the STEG thermal model. A cascaded STEG can be optimized by optimizing two TEGs independently and then combining them together with the radiation exchange to calculate a total efficiency, which is the sum of the two electric power outputs divided by the total intercepted solar power.

When the performance of the optics, absorber, thermal concentration, and TEG are combined, the overall STEG efficiency can be calculated. As with TEGs, the cascaded STEG devices outperform segmented STEG devices. Figure 5 shows the STEG efficiency as a function of geometric optical concentration for the four configurations discussed above. The bismuth telluride STEGs level off quickly once the concentration is enough to push the operating temperature to the material's limit of 250 °C. After that point, the efficiency only grows very slowly with concentration, as the radiation losses become negligible at higher concentrations. The cascaded STEG benefits from its dual-current degree of freedom, but it also benefits from the fact that the midplane acts as a radiation shield, reducing absorber losses while increasing the heat flux to the lower TEG by partially absorbing the radiation emitted from the back side of the absorber. The performance of a cascaded STEG without the beneficial radiation shield effects of the midplane is nearly indistinguishable from the performance with the radiation shield effects, especially when the incident flux on the absorber becomes very large and the radiation losses become insignificant (Fig. 5, gray line). The value for a single-stage bismuth telluride STEG without optical concentration ($C_{g,opt} = 1$) is 4.7%, close to previous experimental results.[8] Cascaded

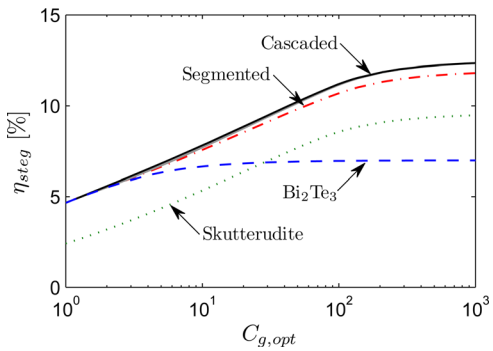

FIG. 5. (Color online) Efficiency for four different STEG architectures: a single-stage bismuth telluride TEG (dashed); a single-stage skutterudite TEG (dotted); a segmented skutterudite and bismuth telluride TEG (dash-dotted); and a cascaded skutterudite and bismuth telluride TEG (solid black). The solid gray line, visible below 20X concentration, shows the cascaded performance without the effect of the midplane acting as a radiation shield.

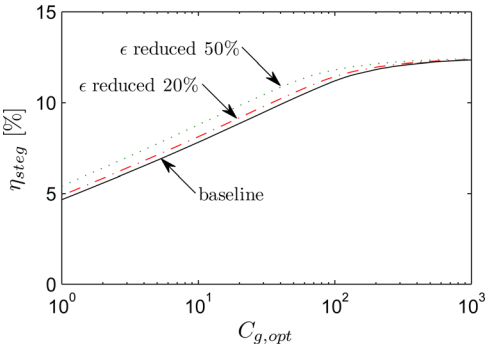

FIG. 6. (Color online) Effect of reduced selective surface emittance on STEG efficiency. Cascaded skutterudite/bismuth telluride STEG efficiencies are plotted as a function of geometric optical concentration.

STEG efficiency can exceed 10% at a geometric optical concentration of 45. At a geometric optical concentration of 100, the skutterudite stage in the cascaded STEG reaches its maximum operating temperature of 600 °C and the gains from increasing concentration lessen.

Two avenues for improving the efficiency of these devices are improving the selective surface and improving the material properties of the thermoelectric materials. The effects of these improvements are shown in Figs. 6 and 7. Improving the emittance at high optical concentrations does not have as strong an effect on the performance of the STEG as improving the material properties, because the optical concentration already suppresses the radiative losses from the absorber surface. Improving the *ZT* of the STEG can come from either making improvements in the current skutterudite and bismuth telluride materials systems or by using other thermoelectric materials systems which could outperform bismuth telluride or skutterudites. Possibilities include, but are not limited to, PbTe, silicon germanium alloys, and half-Heuslers.

IV. CONCLUSION

In conclusion, a model has been developed that calculates the performance of a concentrating STEG. It has been shown that, with these currently existing thermoelectric materials and selective surfaces, the efficiency of cascaded STEGs can theoretically exceed 10%. The hot side of the system is predicted to run at 600 °C or higher if higher-temperature thermoelectric materials are used in systems with optical concentrations exceeding 100 times. The model agrees with experiments performed under little or no optical concentration; concentrating STEG systems whose performance match this model should also be achievable.

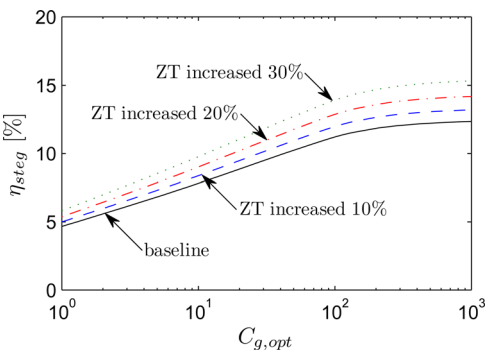

FIG. 7. (Color online) Effect of increased ZT on STEG efficiency. Cascaded skutterudite/bismuth telluride STEG efficiencies are plotted as a function of geometric optical concentration.

ACKNOWLEDGMENTS

This material is partially based upon work supported as part of the Solid State Solar-Thermal Energy Conversion Center (S^3TEC), an Energy Frontier Research Center funded by the U. S. Department of Energy, Office of Science, Office of Basic Energy Sciences under Award Number: DE-SC0001299/DE-FG02-09ER46577 (D.K. and Z.F.R.), the Center for Clean Water and Clean Energy at MIT and KFUPM (K.M.), and the MIT-Masdar program (G.C.).

[1]H. J. Goldsmid, *Applications of Thermoelectricity* (Methuen, London, 1960).
[2]E. Weston, U.S. Patent 389,124 (September 4, 1888).
[3]M. Telkes, J. Appl. Phys. **25**, 765 (1954).
[4]R. Amatya and R. Ram, J. Electron. Mater. **39**, 1735 (2010).
[5]C. L. Dent and M. H. Cobble, in *Proceedings of the Fourth International Conference on Thermoelectric Energy Conversion*, Arlington, TX, March 10–12, 1982, pp. 75–78.
[6]H. Goldsmid, J. Giutronich, and M. Kaila, Sol. Energy **24**, 435 (1980).
[7]S. A. Omer and D. G. Infield, Sol. Energy Mater. Sol. Cells **53**, 67 (1998).
[8]D. Kraemer, B. Poudel, H.-P. Feng, J. Caylor, B. Yu, X. Yan, Y. Ma, X. Wang, D. Wang, A. Muto, K. McEnaney, M. Chiesa, Z. F. Ren, and G. Chen, Nature Mater. **10**, 532 (2011).
[9]G. Chen, J. Appl. Phys. **109**, 104908 (2011).
[10]D. Kraemer, K. McEnaney, M. Chiesa, and G. Chen, "Modeling and optimization of solar thermoelectric generators for terrestrial applications," Sol. Energy (submitted).
[11]B. Poudel, Q. Hao, Y. Ma, Y. Lan, A. Minnich, B. Yu, X. Yan, D. Wang, A. Muto, D. Vashaee, X. Chen, J. Liu, M. S. Dresselhaus, G. Chen, and Z. F. Ren, Science **320**, 634 (2008).
[12]G. J. Snyder and E. S. Toberer, Nature Mater. **7**, 105 (2008).
[13]A. J. Minnich, M. S. Dresselhaus, Z. F. Ren, and G. Chen, Energy Environ. Sci. **2**, 466 (2009).
[14]J. R. Sootsman, D. Y. Chung, and M. G. Kanatzidis, Angew. Chem., Int. Ed. **48**, 8616 (2009).
[15]J. Yang, Q. Hao, H. Wang, Y. C. Lan, Q. Y. He, A. Minnich, D. Z. Wang, J. A. Harriman, V. M. Varki, M. S. Dresselhaus, G. Chen, and Z. F. Ren, Phys. Rev. B **80**, 115329 (2009).
[16]X. Yan, G. Joshi, W. Liu, Y. Lan, H. Wang, S. Lee, J. W. Simonson, S. J. Poon, T. M. Tritt, G. Chen, and Z. F. Ren, Nano Lett. **11**, 556 (2011).
[17]D. M. Rowe, Appl. Energy **8**, 269 (1981).
[18]ASTM, "Reference solar spectral irradiances: Direct normal and hemispherical on 37° tilted surface," Tech. Rep. ASTM Standard No. G 173-03, 2008.
[19]M. F. Modest, *Radiative Heat Transfer,* 2nd ed. (Academic, Boston, 2003).
[20]T. C. Harman, J. Appl. Phys. **29**, 1471 (1958).
[21]M. S. El-Genk and H. H. Saber, AIP Conf. Proc. **608**, 980 (2002).
[22]C. A. Domenicali, Phys. Rev. **92**, 877 (1953).
[23]G. D. Mahan, J. Appl. Phys. **70**, 4551 (1991).
[24]L. Bell, in *Proceedings of the 23rd International Conference on Thermoelectrics*, Adelaide, Australia, July 25–29, 2004.
[25]G. J. Snyder, Appl. Phys. Lett. **84**, 2436 (2004).
[26]J. A. Duffie and W. A. Beckman, *Solar Engineering of Thermal Processes,* 3rd ed. (Wiley, Hoboken, 2006).
[27]G. J. Snyder and T. S. Ursell, Phys. Rev. Lett. **91**, 148301 (2003).
[28]W. Seifert, K. Zabrocki, G. J. Snyder, and E. Mller, Phys. Status Solidi A **207**, 760 (2010).
[29]G. J. Snyder, in *Thermoelectrics Handbook: Macro to Nano*, edited by D. M. Rowe (CRC, New York, 2006), Chap. 9.
[30]B. Sherman, R. R. Heikes, and J. R. W. Ure, J. Appl. Phys. **31**, 1 (1960).